Available online at http://ijim.srbiau.ac.ir/
Int. J. Industrial Mathematics (ISSN 2008-5621)
Vol. 10, No. 2, 2018 Article ID IJIM-00726, 8 pages
Research Article

External and Internal Incompressible Viscous Flows Computation using Taylor Series Expansion and Least Square based Lattice Boltzmann Method

E. Shayan *†

Received Date: 2015-07-17 Revised Date: 2017-11-12 Accepted Date: 2018-05-17

Abstract

The lattice Boltzmann method (LBM) has recently become an alternative and promising computational fluid dynamics approach for simulating complex fluid flows. Despite its enormous success in many practical applications, the standard LBM is restricted to the lattice uniformity in the physical space. This is the main drawback of the standard LBM for flow problems with complex geometry. Several approaches have been developed to remove this drawback of standard LBM. One of these methods is the Taylor series expansion and least squares-based LBM (TLLBM). This method is based on the standard LBM combined with the Taylor series expansion and the least squares approach. The prominent feature of the TLLBM is the fact that the final equation is an explicit form and in essence has no limitation on the mesh structure and lattice model. In the present work, the TLLBM with D2Q9 lattice model is used to simulate 2-D steady incompressible viscous flows (both internal and external) on non-uniform meshes. Four test cases are studied: (i) flow past a circular cylinder with a non-uniform O-type mesh; (ii) flow in a rectangular lid driven cavity with a non-uniform H-type mesh; and (iii) flow over a backward- facing step. It was found that this model could give very accurate results for both the internal and external flows.

Keywords : Lattice-Boltzmann method; Circular cylinder; Lid driven cavity; Backward-facing step.

1 Introduction

In recent years, the lattice Boltzmann method (LBM) [1, 2] has been used as a computational fluid dynamics (CFD) approach for simulating fluid flows. Unlike conventional numerical schemes based on discretization of macroscopic continuum equations, the LBM is based on microscopic models and mesoscopic kinetic equations. The major advantages of the LBM are the explicit feature of the governing equation, easy for parallel computation, and simple implementation of boundary conditions on curved boundaries. The LBM is usually applied on a uniform mesh in the Cartesian coordinate system, and cannot be directly applied to problems with complex geometry. This greatly limits its application to solve practical problems. On the other hand, most flow problems involve complex geometry and need to use the non-uniform mesh to capture the thin

*Corresponding author. e_shayan_1@yahoo.com, Tel: +98(914)4825986
†Department of Mechanical Engineering, Urmia University, Urmia, Iran.

boundary layer.

The first lattice Boltzmann model [1, 2] was a direct transcription from the lattice gas automata (LGA). The Boolean variables in the LGA [3, 4] were replaced by a real-number single particle distribution function. This replacement eliminates the intrinsic stochastic noise in LGA and subsequently enhances the computational efficiency. The current lattice Boltzmann models adopt the simple relaxation BGK model [5] for the collision operator, which further simplifies the algorithm, and more importantly, eliminates the lack of Galilean invariance and the dependence of pressure on velocity [6, 7]. It has been proved that the lattice Boltzmann equation recovers the Navier-Stokes equation using the Chapman-Enskog expansion [6, 7].

The LBM suffers from the drawback of its essential dependence on the lattice-uniformity. This feature of lattice-uniformity is not theoretically necessary to be kept because the distribution functions are continuous in physical space. To remove this drawback of standard LBM, the following four ways have been developed: (i) the interpolation supplemented LBM proposed by He and Doolen [8]. In this method, interpolation is applied at every time step in order to obtain the density distribution function at the grid points. Therefore, it needs much more computational costs as compared to the standard LBM; (ii) the differential LBM, which is based on the solution of a partial differential equation. For complex problems, this scheme can be solved by traditional CFD methods; (iii) the grid refinement technique, which was first presented by Fillipova and Hanel [9] and further improved by Mie et al [10]. This technique is based on the conventional adaptive mesh refinement method; (iv) the Taylor series expansion and least squares-based LBM (TLLBM), which was first proposed by Shu et al [11]. This method is based on the standard LBM with introduction of the Taylor series expansion and the least squares approach. The salient feature of this method is the fact that the final equation is an explicit form and essentially has no limitation on the mesh structure and lattice model.

In the present work, the TLLBM with D2Q9 lattice model is used to simulate 2-D steady incompressible viscous (internal and external) flows on non-uniform meshes. Three test cases are studied: (a) flow past a circular cylinder with a non-uniform O-type mesh; (b) flow in a rectangular lid driven cavity with a non-uniform H-type mesh; (c) flow over a backward- facing step. It was found that very accurate results could be obtained by using this model.

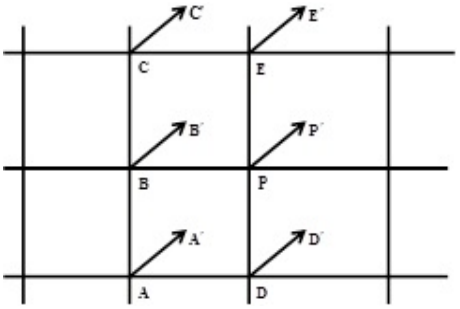

Figure 1: Configuration of particle movement along the direction on a non-uniform mesh.

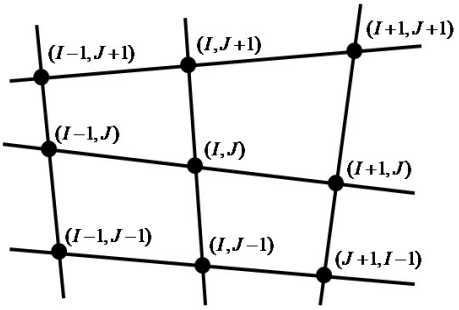

Figure 2: Configuration of neighboring points around the point (I, J).

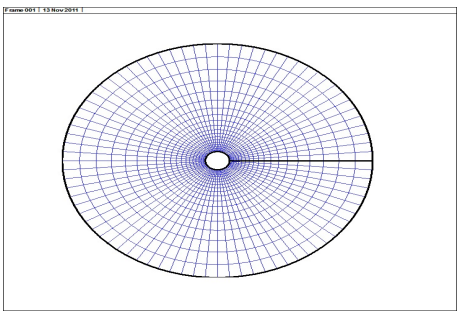

Figure 3: Computational mesh for flow around the circular cylinder

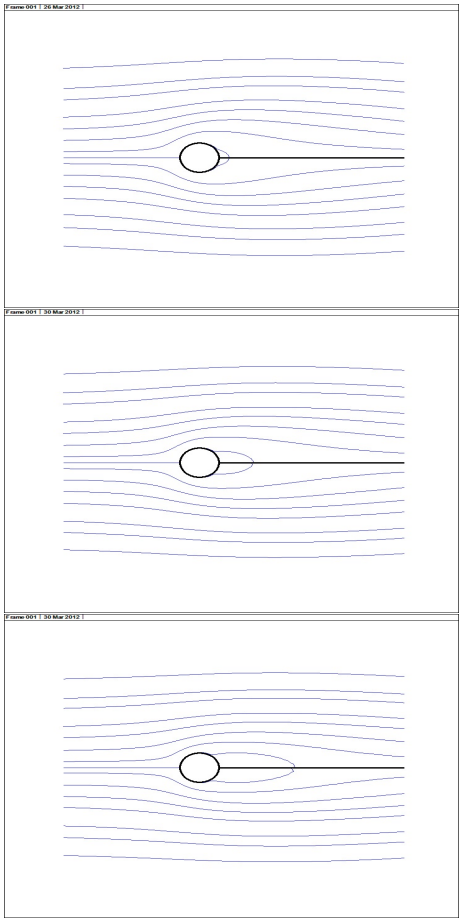

Figure 4: Streamlines around the circular cylinder for different Reynolds numbers: (a) = 10, (b) = 20, (c) = 40.

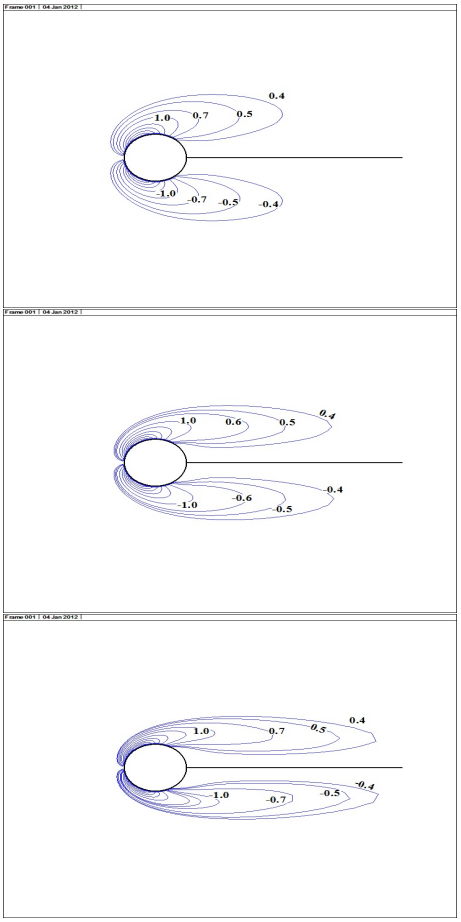

Figure 5: Vorticity contours around the circular cylinder for different Reynolds numbers: (a) = 10, (b) = 20, (c) = 40.

2 Governing equations

The two-dimensional Navier-Stokes equations for an incompressible fluid flow can be written as,

$$\nabla \cdot \mathbf{u} = 0 \tag{2.1}$$

$$\partial_t \mathbf{u} + (\mathbf{u} \cdot \nabla)\mathbf{u} = -\frac{1}{\rho}\nabla p + \nu \nabla^2 \mathbf{u} \tag{2.2}$$

where $\mathbf{u}$ is the velocity vector, ρ represents density, p is pressure and ν denotes kinematic viscosity. These equations along with the appropriate boundary conditions are solved to obtain the required flow properties.

3 Taylor series expansion and least squares-based LBM (TLLBM)

The TLLBM is based on the fact that the density distribution function is a continuous function in physical space and can be used with any mesh systems. The 2-D, standard LBM with Bhatnagar-Gross-Krook (BGK) approximation can be written as

$$f_\alpha(x + e_{\alpha x}\delta t, y + e_{\alpha y}\delta t, t + \delta t) = f_\alpha(x, y, t) + \frac{1}{\tau}\left[f_\alpha^{eq}(x, y, t) - f_\alpha(x, y, t)\right], \quad (\alpha = 0, 1, \cdots, N) \tag{3.3}$$

where τ is the single relaxation time (SRT); f_α is the density distribution function along the α direction and f_α^{eq} is its corresponding equilibrium state δt is the time step and $\mathbf{e}_\alpha(e_{\alpha x}, e_{\alpha y})$ is the particle velocity in the direction; and N is the number of discrete particle velocities. The macroscopic variables are defined as

$$\rho = \sum_{\alpha=0}^{N} f_\alpha, \ \rho u = \sum_{\alpha=0}^{N} f_\alpha e_{\alpha x}, \ \rho v = \sum_{\alpha=0}^{N} f_\alpha e_{\alpha y}. \tag{3.4}$$

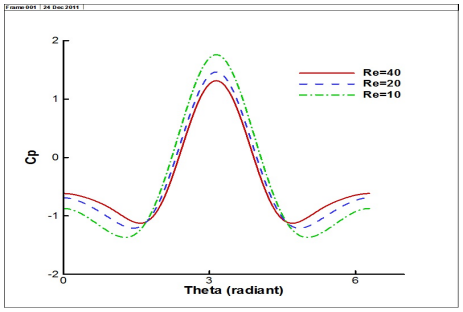

Figure 6: Pressure distribution on the cylinder wall for different Reynolds numbers.

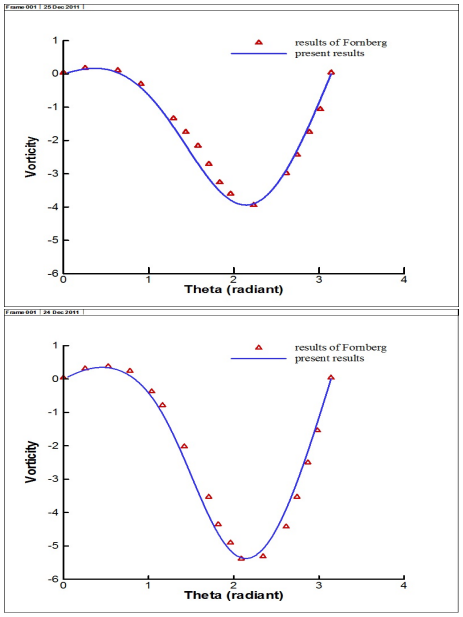

Figure 7: Vorticity distribution on the cylinder wall for different Reynolds numbers. (a) = 20, (b) = 40.

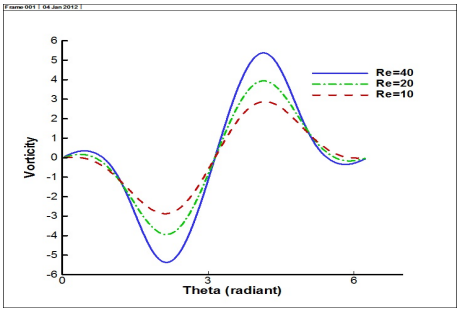

Figure 8: Vorticity distribution on the cylinder wall for different Reynolds numbers.

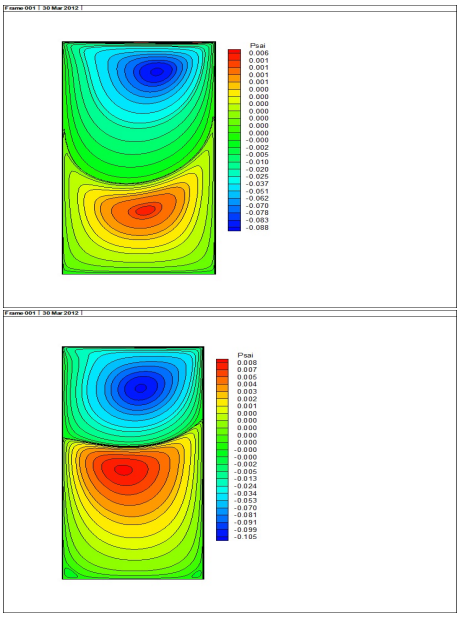

Figure 9: Streamlines of the flow in a rectangular lid-driven cavity at (a) = 100, (b) = 400.

The pressure is directly computed from the ideal gas equation of state

$$p = \rho {c_s}^2 \tag{3.5}$$

where c_s is the speed of sound. Suppose that a particle is initially at the grid point (x, y, t). Along the α direction, this particle will stream to the position $(x + e_{\alpha x}\delta t, y + e_{\alpha y}\delta t, t + \delta t)$. For a uniform lattice, $\delta x = e_{\alpha x}\delta t$ and $\delta y = e_{\alpha y}\delta t$. So, $(x + e_{\alpha x}\delta t, y + e_{\alpha y}\delta t)$ is exactly on the grid point. In other words, Eq. (3.3) can be used to update the density distribution functions exactly at the grid points. However, for a non-uniform grid, $(x + e_{\alpha x}\delta t, y + e_{\alpha y}\delta t)$ is usually not at the grid point $(x + \delta x, y + \delta y)$. To get the density distribution function at the grid point $(x + \delta x, y + \delta y)$ and the time level $t + \delta t$, we need to apply the Taylor series expansion or other interpolation techniques such as the one used by He and Doolen [8]. Here, the Taylor series expansion is used. Note that the time level for the position $(x + e_{\alpha x}\delta t, y + e_{\alpha y}\delta t)$ and the grid point $(x+\delta x, y+\delta y)$ is the same, that is, $t + \delta t$. So, the expansion in the time direction is not necessary.

As shown in Figure 1, it can be seen that along the direction, the particles at five mesh points P, B, C, D and E at the time level t will move to the new positions P', B', C', D' and E' at the time level $t + \delta t$. The density distribution functions at these new positions can be computed through

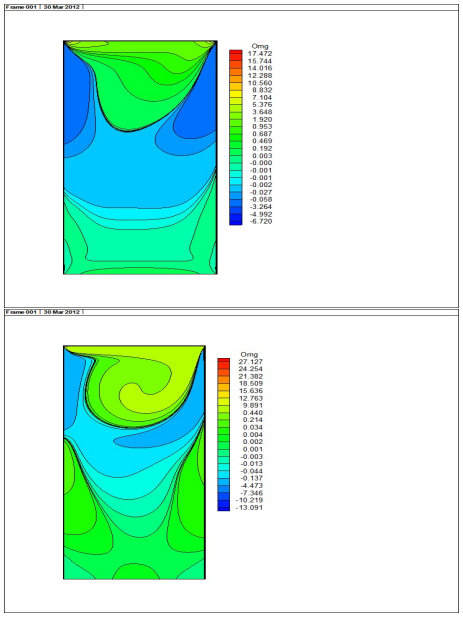

Figure 10: Vorticity contours of the flow in a rectangular lid-driven cavity at (a) = 100, (b) = 400.

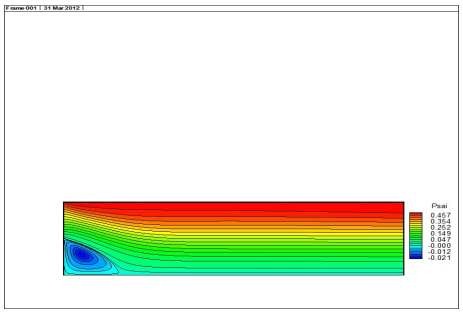

Figure 11: Streamlines for the flow in a channel with a backward-facing step at = 100.

Eq. (3.3), which are given as,

$$f_\alpha(\Phi', t+\delta t) = f_\alpha(\Phi, t) + \frac{f_\alpha^{eq}(\Phi, t) - f_\alpha(\Phi, t)}{\tau} \tag{3.6}$$

where Φ denotes P, B, C, D and E. Using Taylor series expansion, $f_\alpha(\Phi', t+\delta t)$ in the equation set (3.6) can be approximated by the function and its derivatives at the mesh point P. As a result, the equation set (3.6) can be reduced to

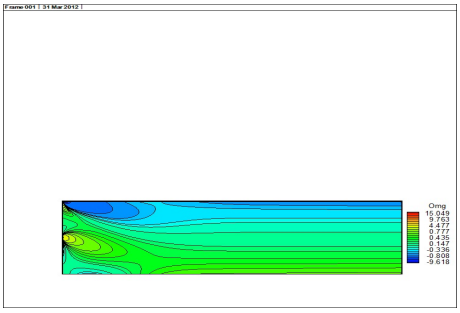

Figure 12: Vorticity contours for the flow in a channel with a backward-facing step at = 100.

$$\begin{aligned} & f_\alpha(P, t+\delta t) + \\ & \Delta x_\Phi \frac{\partial f_\alpha(P, t+\delta t)}{\partial x} + \Delta y_\Phi \frac{\partial f_\alpha(P, t+\delta t)}{\partial y} + \frac{1}{2}(\Delta x_\Phi)^2 \\ & \frac{\partial^2 f_\alpha(P, t+\delta t)}{\partial x^2} + \frac{1}{2}(\Delta y_\Phi)^2 \frac{\partial^2 f_\alpha(P, t+\delta t)}{\partial y^2} \\ & + \Delta x_\Phi \Delta y_\Phi \frac{\partial^2 f_\alpha(P, t+\delta t)}{\partial x \partial y} \\ & = f_\alpha(\Phi, t) + \frac{1}{\tau}\left[f_\alpha^{eq}(\Phi, t) - f_\alpha(\Phi, t)\right] \end{aligned} \tag{3.7}$$

where $\Delta x_\Phi = x_\Phi + e_{\alpha x}\delta t - x_P$ and $\Delta y_\Phi = y_\Phi + e_{\alpha y}\delta t - y_P$. With the above definitions, the equation set (3.6) can be written as

$$g_i = \{s_i\}^T\{V\} = \sum_{j=1}^{6} s_{i,j} V_j, \quad i = P, A, B, C, D, E \tag{3.8}$$

where

$$\begin{aligned} & g_i = f_\alpha(x_i, y_i, t) + \frac{1}{\tau}\left[f_\alpha^{eq}(x_i, y_i, t) - f_\alpha(x_i, y_i, t)\right], \\ & \{s_i\}^T = \left\{1, \Delta x_i, \Delta y_i, (\Delta x_i)^2/2, (\Delta y_i)^2/2, \Delta x_i \Delta y_i\right\}, \\ & \{V\} = \{f_\alpha, \partial f_\alpha/\partial x, \partial f_\alpha/\partial y, \\ & \qquad \partial^2 f_\alpha/\partial x^2, \partial^2 f_\alpha/\partial y^2, \partial^2 f_\alpha/\partial x \partial y\}^T, \end{aligned}$$

$s_{i,j}$ is the jth element of the vector $\{s_i\}^T$ and V_j is the jth element of the vector $\{V\}$. The target is to find the first elements of $\{V\}$, i.e., $V_1 = f_\alpha(P, t+\delta t)$. Equation system (3.8) can be put in to the following matrix form

$$[S]\{V\} = \{g\} \tag{3.9}$$

Note that the matrix $[S]$ only depends on the coordinates of mesh points, which can be computed once and stored for the application of Eq. (3.9)

at all time levels. In practical applications, it was found that the matrix $[S]$ might be singular or ill-conditioned. To overcome this difficulty and make the method be more general, we propose the following least squares-based LBM. At each point, we can define an error in terms of Eq. (3.8), that is,

$$\mathrm{err}_i = g_i - \sum_{j=1}^{6} s_{i,j} V_j, \quad i = 0, 1, 2, \cdots, M. \tag{3.10}$$

The square sum of all the errors are defined as

$$E = \sum_{i=0}^{M} \mathrm{err}_i^2 = \sum_{i=0}^{M} \left(g_i - \sum_{j=1}^{6} s_{i,j} V_j \right)^2. \tag{3.11}$$

To minimize the error E, we need to set $\partial E/\partial V_j = 0$, $j = 1, 2, \cdots, 6$, which leads to

$$[S]^T [S]\{V\} = [S]^T \{g\} \tag{3.12}$$

Clearly, when the coordinates of mesh points are given, and the particle velocity and time step size are specified, the matrix $[S]$ is determined. Then from Eq. (3.12), we obtain

$$\{V\} = \left([S]^T [S] \right)^{-1} [S]^T \{g\} = [A]\{g\}. \tag{3.13}$$

Note that $[A]$ is a $6 \times (M+1)$ dimensional matrix. From Eq. (3.13), we have

$$f_\alpha(x_0, y_0, t + \delta t) = V_1 = \sum_{k=1}^{M+1} a_{1,k} g_{k-1}, \tag{3.14}$$

where $a_{1,k}$ are the elements of the first row of matrix $[A]$, which are pre-computed before the LBM is applied. Note that, we just need to compute these coefficients once and store them for use in all the time levels.

4 D2Q9 lattice model

An important feature of TLLBM is that it can be applied to any lattice velocity model. In this work, the D2Q9 model is used. The equilibrium density distribution function f_α^{eq} with D2Q9 model can be written as

$$f_\alpha^{eq} = \rho w_\alpha \left[1 + \frac{3}{c^2}(\mathbf{e}_\alpha \cdot \mathbf{u}) + \frac{9}{2c^4}(\mathbf{e}_\alpha \cdot \mathbf{u})^2 - \frac{3}{2c^2}(\mathbf{u} \cdot \mathbf{u}) \right] \tag{4.15}$$

where $c = \delta x/\delta t$, w_α is the weighting factor and defined as,

$$w_\alpha = \begin{cases} 4/9, & i = 0 \\ 1/9, & i = 1, 3, 5, 7 \\ 1/36, & i = 2, 4, 6, 8 \end{cases}$$

and $\mathbf{e}\alpha(e_{\alpha x}, e_{\alpha y})$ is the discrete velocity set given by

$$\mathbf{e}_\alpha = \begin{cases} (0,0), & \alpha = 0 \\ (\cos\theta\alpha, \sin\theta\alpha)c, & \alpha = 1, 3, 5, 7 \\ \sqrt{2}(\cos\theta_\alpha, \sin\theta_\alpha)c, & \alpha = 2, 4, 6, 8. \end{cases}$$

where $\theta_\alpha = (\alpha - 1)\pi/4$. The speed of sound in this model is $c_s = c/\sqrt{3}$ and the corresponding viscosity in the Navier-Stokes Eq. (2.2) is defined as

$$\nu = (\tau - 1/2){c_s}^2 \delta t. \tag{4.16}$$

As noted above, the TLLBM has mesh-free feature and it can be applied on any non-uniform meshes. However, for simplicity in determining the coordinates of the mesh points in this work, structured grids have been used. For convenience M is taken to be 8. As shown in figure 2, for an internal mesh point (I, J), we have 8 neighboring points. Note that the configuration of 9 mesh points (see figure 2) is applied in all lattice directions ($\alpha = 1, 2, \cdots, 8$).

Figure 6 shows the pressure distribution on the cylinder wall for different Reynolds numbers. The pressure is expressed in its nondimensional form,

$$C_P = (P - P_\infty)/\frac{1}{2}\rho U_\infty^2 \tag{4.17}$$

The highest pressure is observed at the front stagnation point ($\theta = 180°$). The location of the lowest pressure does not occur at the rearmost point of the cylinder. It moves upstream as the Reynolds number increases.

Figure 7 shows vorticity distribution on the cylinder wall for two Reynolds numbers of 20, and 40. The numerical results of Fernberg [12] by solving

Navier-Stokes equations are also shown in this figures for comparison.
Figure 8 shows the vorticity distribution on the cylinder wall for different Reynolds numbers.

5 Boundary conditions

In the present study, four kinds of boundary conditions have been implemented. The first one is on the rigid walls, where the no-slip (the well-known bounce back) condition is employed. This treatment is independent of the direction, giving more conveniences in treating complicated boundary problems. The second one is on the far field boundary, where it is reasonably assumed that the flow is a potential one with the density distribution function at its equilibrium state. The third one is the periodic boundary condition that is applied on the cut line for the O-type grid. The fourth one is the inlet and outlet boundary conditions that are applied on the inlet and outlet of the channel with a backward-facing step.

6 Results and Discussions

In this study, both internal and external flows are studied using TLLBM with D2Q9 discrete velocity model. The details of the test cases and the results are described below.

6.1 Flow past the circular cylinder

Numerical simulations were carried out for three small Reynolds numbers of 10, 20 and 40, based on the upstream velocity U_∞ and the diameter of the cylinder D. The reported data are obtained from simulations on a 181×121 and a 241×181 O-type grid for Reynolds numbers of 10, 20 and 40, respectively. A typical mesh is shown in figure 3. The far field boundary is set at 25.5D and 50.5D away from the center of the cylinder.

Figures 4 and 5 show the streamlines and vorticity contours, respectively. In both cases, a pair of stationary recirculating eddies develops behind the cylinder. The length of the recirculating region, L, from the rearmost point of the cylinder to the end of the wake, increases linearly with the Reynolds number.

6.2 Flow in a rectangular lid-driven cavity

In this case, the top lid of the cavity moves from left to right with a constant velocity U. Here, we study the flow with = 100 and = 400, where = $UL/$ is the

Reynolds number based on the lid velocity and the small length of the rectangular cavity. Non-uniform meshes of 131×65 for = 100, and 261×101 for = 400 are used.

Initially a constant density $\rho = 1$ is prescribed in the whole field, and the velocities in the interior of the cavity were set to zero. On the top, the x-component velocity (U) was set to 0.15, and the y-component velocity was zero. At the end of each time step, the density distribution function f_α at the top wall was set to the equilibrium state. Note that, all the results obtained in this work were normalized by the top lid velocity U. The whole halfway wall bounce back boundary conditions are used on the other three stationary walls.

Figure 9 shows the streamlines at Reynolds numbers of 100 and 400. The effect of the Reynolds number on the flow pattern and the structure of the steady recirculating eddies is clearly observed in this figure. From this figure, one can easily see that the scale of the primary vortex increases with the Reynolds number. Figure 10 shows the vorticity contours inside the cavity.

6.3 Flow over a backward-facing step

In this case, the flow in a channel with a backward-facing step is investigated. A non-uniform mesh of 513×51 is used. The flow geometry used in this problem, is described below.

The upstream channel height is 0.5 and the downstream channel height is 1 and upstream velocity is $U_\infty = 0.2$. Here, we study the flow with = 100. Figures 11 and 12 show the streamlines and vorticity contours, respectively.

7 Conclusions

An explicit mesh-free LBM (i.e., TLLBM) was used in this paper to simulate various (both external and internal) 2-D viscous incompressible

flows. Theoretical analysis for a one-dimensional case showed that the present method could recover the Navier-Stokes equations with second order of accuracy [11]. The beauty of the present method is that it still keeps the local and explicit features of the standard LBM. The other advantage of the present method is that it is easy for application to flow problems with complex geometry. The results prove the efficiency of the present method.

References

[1] G. McNamara, G. Zanetti, Use of the Boltzmann equation to simulate lattice-gas automata, *Phys Rev Lett* 61 (1988) 2332-2335.

[2] Fj. Higuera, J. Jemenez, Boltzmann approach to lattice gas simulations, *Europhys Lett* 9 (1989) 663-668.

[3] U. Frisch, B. Hasslacher, Y. Pomeaue, Lattice-gas automata for the Navier-Stokes equation, *Phys Rev Lett* 56 (1986) 1505-1512.

[4] S. Wolfram, Cellular automaton fluid 1: Basic theory, *J Stat Phys* 45 (1986) 471-479.

[5] PL. Bhatnagar, EP. Gross, M. Krook, A model for collision processes in gases. I. Small amplitude processes in charged and neutral one-component system, *Phys Rev*94 (1954) 511-519.

[6] H. Chen, S. Chen, WH Matthaeus, Recovery of the Navier-Stokes equations using a lattice-gas Boltzmann method, *Phys Rev A* 45 (1992) 339-342.

[7] YH. Qian, D. d'Humières, P Lallemand, Lattice BGK models for the NavierStokes equation, *Europhys Lett* 17 (1992) 479-489.

[8] X. He, GD. Doolen, Lattice Boltzmann method on curveilinear coordinates system: Flow around a circular cylinder, *J Comput Phys* 134 (1997) 306-315.

[9] O. Filippova, D. Hanel, Grid refinement for lattice-BGK models, *J Comput Phys* 147 (1998) 219-228.

[10] R. Mei, LS. Luo, W. Shyy, An accurate curved boundary treatment in the lattice Boltzmann method, *J Comput Phys* 155 (1999) 307-330.

[11] C. Shu C, YT. Chew, XD. Niu, Least-squares-based lattice Boltzmann method: A meshless approach for simulation of flows with complex geometry, *Phys Rev E* 64 (2001) 45-70.

[12] B. Fornberg, A numerical study of steady viscous flow past a circular cylinder, *J Fluid Mech* 98 (1980) 819-855.

Elnaz Shayan is a Ph.D. candidate within the Department of Mechanical Engineering at the Urmia University, Urmia, Iran. She received her M.Sc degree from Urmia University of Technology, Urmia, Iran, in 2011. Her research interests are in the areas of Computational fluid dynamics (CFD).